Studies of an Fe_9 Tridiminished Icosahedron

Evangelos I. Tolis,[a] Larry P. Engelhardt,[b] Pamela V. Mason,[a] Gopalan Rajaraman,[a] Koichi Kindo,[d] Marshall Luban,*[b] Akira Matsuo,[d] Hiroyuki Nojiri,*[c] James Raftery,[a] Christian Schröder,[e] Grigore A. Timco,[a] Floriana Tuna,[a] Wolfgang Wernsdorfer,[f] and Richard E. P. Winpenny*[a]

Abstract: The synthesis and structural characterization of a nonanuclear Fe^{III} cage complex is reported. The nine iron centers in $[Fe_9(\mu_3\text{-}O)_4(O_3PPh)_3(O_2CCMe_3)_{13}]$ lie on the vertices of an incomplete icosahedron, with the P atoms of triphenylphosphonate at the other three vertices. The paramagnetic core therefore describes a tridiminished icosahedron. Magnetic studies suggest an $S=1/2$ ground state for the molecule. Analysis of exchange paths and the susceptibility data point to the interpretation that the cluster can be divided into two nearly decoupled sections: an $\{Fe_6O_3\}$ section, with an $S=0$ ground state, in which three oxo-centered triangles bound a central triangle that is not oxo-centered; and an $\{Fe_3O\}$ triangle with $S=1/2$. The analysis of the susceptibility data leads to a Heisenberg model based on three significant antiferromagnetic exchange interactions, with values of 173.7 cm^{-1} in the $\{Fe_3O\}$ triangle, and 30.9 and 19.1 cm^{-1} within the $\{Fe_6O_3\}$ section, while the exchange between them is <1 cm^{-1}. With these assignments, the theoretical low-temperature differential susceptibility is also in very good agreement with measurements up to 50 T. Magnetic measurements in the milli-kelvin range reveal striking hysteresis loops and magnetization reversals associated with a Landau–Zener–Stückelberg (LZS) transition as enhanced by the occurrence of a phonon bottleneck.

Keywords: cage compounds · iron · molecular magnetism · phosphonate ligands · X-ray diffraction

[a] Dr. E. I. Tolis, Dr. P. V. Mason, Dr. G. Rajaraman, Dr. J. Raftery, Dr. G. A. Timco, Dr. F. Tuna, R. E. P. Winpenny
School of Chemistry, The University of Manchester
Oxford Road, Manchester, M13 9PL (UK)
Fax: (+44)161-275-4616
E-mail: richard.winpenny@man.ac.uk

[b] L. P. Engelhardt, Prof. Dr. M. Luban
Department of Physics & Astronomy, Ames Laboratory
Iowa State University, Iowa, IA 50011 (USA)
Fax: (+1)515-294-0689
E-mail: luban@ameslab.gov

[c] Prof. Dr. H. Nojiri
Institute for Material Research, Tohoku University
Katahira 2–1–1, Sendai, 980–8577 (Japan)
E-mail: nojiri@imr.tohoku.ac.jp

[d] Prof. K. Kindo, Dr. A. Matsuo
Institute for Solid-State Physics, University of Tokyo
Kashiwanoha 5–1–5, Kashiwa 277–8581 (Japan)
Fax: (+81)22-215-2016

[e] Prof. Dr. C. Schröder
Department of Electrical Engineering and Computer Science
University of Applied Sciences, Bielefeld, 33602 (Germany)

[f] Dr. W. Wernsdorfer
Laboratoire Louis Néel - CNRS, BP 166
25 Avenue des Martyrs, 38042 Grenoble Cedex 9 (France)

Introduction

The Platonic solids[1] underpin much of our discussion of solid geometry, for example, for those of us making polymetallic complexes they often provide the starting point for the description of structures.[2] For example, many metal cages are based on tetrahedra, octahedra or cubes, but, in contrast, the twelve-vertex Platonic solids—the pentagonal dodecahedron and the icosahedron—remain unknown for paramagnetic ions. From a magnetic viewpoint these polyhedra would be fascinating; for example an icosahedron with paramagnetic ions at the vertices interacting via nearest-neighbor antiferromagnetic exchange is predicted to show a sudden metamagnetic transition when an increasing external field H exceeds a critical value H_c, and exhibit distinctive metastable behavior on the down-cycle.[3] Although we have not yet made an icosahedron, the structure reported is of interest. The nine Fe centers span what is known in the mathematics literature as a "tridiminished icosahedron". We find that the body of diverse experimental data reported here can be consistently interpreted, in such a way that the present system is characterizable magnetically in terms of a six-spin fragment and a three-spin fragment that are very

weakly coupled. At very low temperatures the large and small fragments have total spin $S=0$ and $S=1/2$, respectively. Moreover, this picture of the system is also supported by an examination of the possible exchange pathways.

We have been exploring displacement reactions where carboxylate ligands in a pre-formed metal cage can be replaced by a phosphonate ligand.[4] Specifically, oxo-centered iron(III) triangles react with a range of phosphonates to give tetra-, hexa-, hepta-, and tetradecanuclear iron(III) cages. In each of these compounds iron triangles are largely retained, and the chemistry is based on discrete triangles linked through phosphonates and, on occasion, individual Fe[III] ions. The triangles studied[4] have the general formula $[Fe_3O(O_2CR)_6(H_2O)_3]X$, where a range of R groups were studied (e.g. Me, Ph, CMe$_3$) and X=chloride or nitrate. Here we discuss the unusual, and more symmetric, complex that results if both the bound carboxylate and the counterion are pivalate (trimethylacetate). Nonanuclear Fe[III] cages have previously been reported with polycarboxylates such as citrate[5] and 2-hydroxy-1,3-*N,N,N′,N′*-diaminopropanetetraacetate.[6] Thompson and co-workers has also made a 3×3 Fe[III] grid.[7]

Results

Structural studies: If $[Fe_3O(O_2CCMe_3)_6(H_2O)_3](O_2CCMe_3)$ is allowed to react with one equivalent of phenylphosphonic acid, $[Fe_9(\mu_3\text{-}O)_4(O_3PPh)_3(O_2CCMe_3)_{13}]$ (**1**) is formed in 68% yield. The structure (Figure 1) shows that the nonanuclear cage contains oxo-centered {Fe$_3$} triangles. One discrete triangle (Fe1, Fe2, and Fe8) in **1** has the same {Fe$_3$O}

Figure 1. The structure of **1** in the crystal. Shading: Fe: cross-hatched circle; P: diagonal top right-bottom left; O: light shading; C: drawn as lines.

core as in the starting material, but the remaining six iron-(III) centers occupy the vertices of three oxo-centered triangles bounding a central triangle (with Fe5, Fe6, and Fe7 at its vertices) that is not oxo-centered. The discrete {Fe$_3$O} fragment is bound to the {Fe$_6$O$_3$} unit by three phenylphosphonate ligands, which adopt the 5.221-bridging mode (Harris notation[8]). Each of the three phosphonates bridge one edge of the {Fe$_3$O} triangle, in a manner equivalent to that adopted by the carboxylate in the starting material, but each of the three O atoms also bind to a separate Fe[III] site of the {Fe$_6$O$_3$} unit.

A clearer description of the structure can be achieved if we remove all atoms except the Fe and P sites (Figure 2).

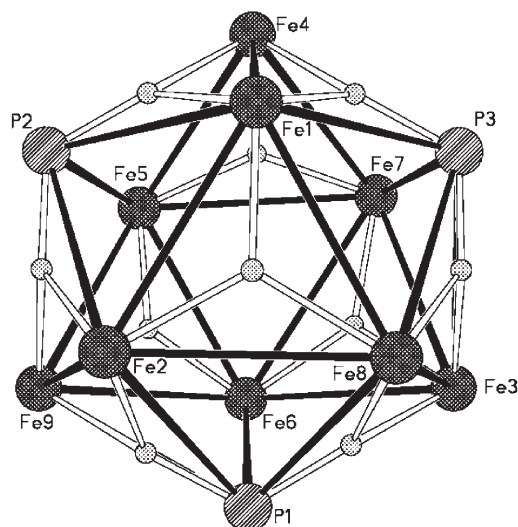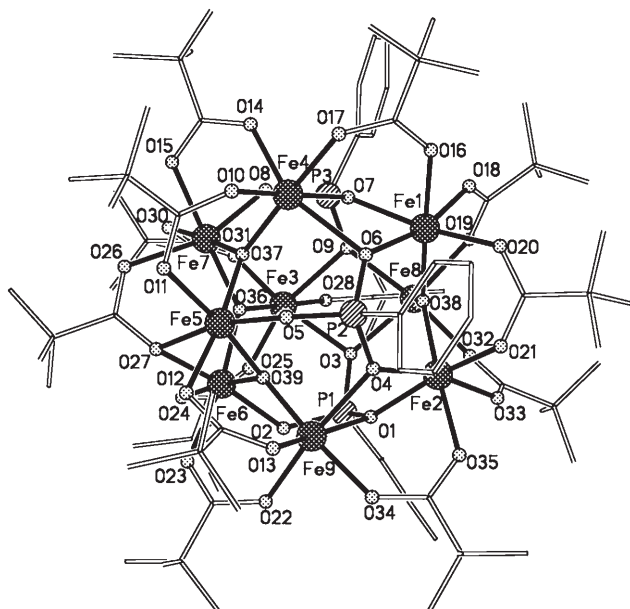Figure 2. The icosahedral core of **1**. Unlabeled atoms are μ_3-O bridges at the centers of {Fe$_3$} triangles.

Each P center has five Fe[III] nearest neighbors, and each Fe[III] site has five nearest neighbors (either four Fe and one P, or three Fe and two P); the Fe$_9$P$_3$ core is therefore an icosahedron. Sadly the paramagnetic sites have a lower symmetry; the Fe$_9$ core lies on the vertices of a particular Johnson solid[9]—the tridiminished icosahedron—which retains only threefold symmetry, albeit non-crystallographic. On the basis of the different crystallographic symmetries of the nine Fe[III] one can anticipate that four distinct exchange interactions will be necessary (Figure 2).

It is the pentanucleating 5.221-bridging mode adopted by the phosphonates—creating a pentagon of Fe[III] sites—that seems to be responsible for the icosahedral symmetry. The pivalate ligands are, with one exception, 2.11 bridging. Nine lie on edges of triangles, while three link between the discrete triangle and the {Fe$_6$O$_3$} triangular fragment. The thirteenth pivalate provides the only distortion from threefold symmetry. This binds in a 3.21 mode to the non-oxo-centered triangle. O27 bridges one edge (Fe5 and Fe6), while O26 binds to the third Fe of the triangle (Fe7).

Magnetic studies: Although the idealized magnetic icosahedron has not yet been formed, the magnetic properties of **1** remain intriguing—especially with the possibility of considerable spin frustration given the large number of paramagnetic triangles present. Studies of paramagnetic triangles have a considerable history, for example, Welo performed measurements on oxo-centered carboxylate triangles in the late 1920s—which allowed the triangular structure to be deduced.[10] The field has been reviewed by Cannon and White.[11]

The experimental value of $\chi_M T$ (where χ_M is the molar magnetic susceptibility) decreases smoothly from a room-temperature value of about 12.7 emu K mol⁻¹ (Figure 3). The
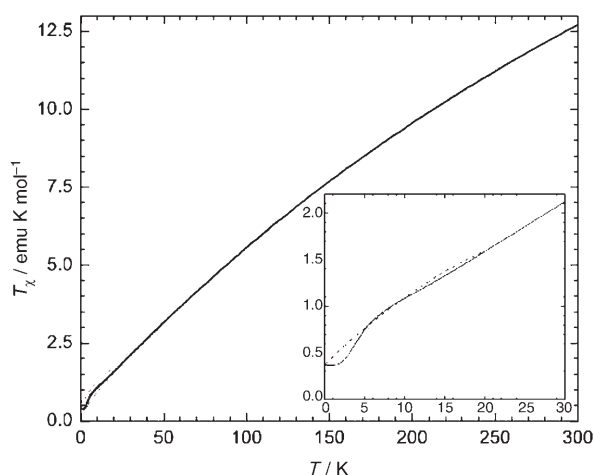

Figure 3. Magnetic behaviour of **1** shown as a plot of $\chi_M T$ against T. Measured data: open circles. Calculated values based on the quantum model for the exchange constants given in the text: full line. Inset: expansion of low T regime. Dashed line is a least-squares fit to the measured data using a polynomial in T of degree two.

room-temperature value is considerably smaller than the Curie value (39.4 emu K mol⁻¹ assuming $g = 2$), showing that the exchange is moderately strong, and antiferromagnetic. Referring to Figure 2 the field-free Hamiltonian may be written as given in Equation (1).

$$H = -J_a(S_1 \cdot S_2 + S_1 \cdot S_8 + S_2 \cdot S_8) - J_b(S_3 \cdot S_6 + S_3 \cdot S_7 + S_6 \cdot S_9 + S_5 \cdot S_9 + S_4 \cdot S_5 + S_4 \cdot S_7) - J_c(S_5 \cdot S_6 + S_5 \cdot S_7 + S_6 \cdot S_7) - J_2(S_3 \cdot S_8 + S_2 \cdot S_9 + S_1 \cdot S_4) \tag{1}$$

Direct diagonalization of the Hamiltonian is not possible given the size of the matrices involved (ca. 10^7 rows and columns). Therefore we have adopted a slightly circuitous route to fitting the magnetic data.

First we performed a series of DFT calculations on a model structure of **1**, $[Fe_9(\mu_3\text{-}O)_4(O_3CH)_3(O_2CCH_3)_{13}]$, using Gaussian 98,[12] with the hybrid B3LYP functional together with Ahlrich's TZV basis set but we required $J_a = J_b = J_c = J_1$. This greatly reduces the computational time as we only

need two exchange interactions and hence only the energies of three spin configurations have to be calculated; those used are shown in Figure 4. Similar procedures have been
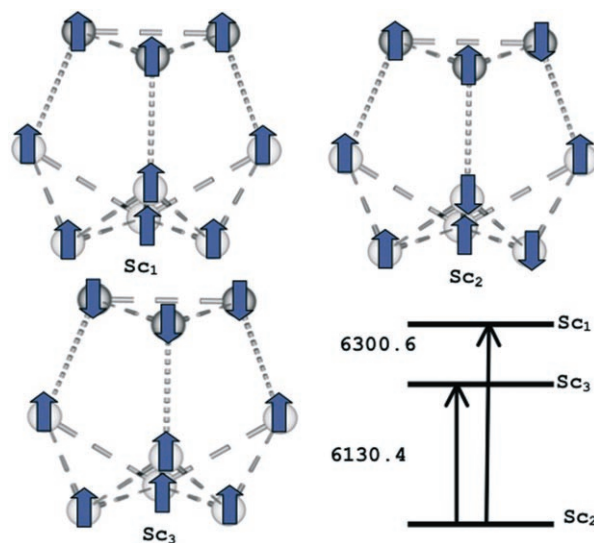

Figure 4. The spin configurations chosen to calculate the exchange interactions in **1**, and their relative energies in cm⁻¹.

found to give good numerical estimates of J values in previous work.[13] The energy gaps between the three spin configurations are related to the exchange interactions by Equations (2) and (3):

$$(E_{sc1} - E_{sc2})/15 = -8J_1 - 2J_2 \tag{2}$$

$$(E_{sc1} - E_{sc3})/15 = -3J_2 \tag{3}$$

The calculations give $J_1 = -51.6$ cm⁻¹ and $J_2 = -3.8$ cm⁻¹.

As the DFT calculation suggested J_2 is small we felt justified in adopting the choice $J_2 = 0$, that is, reducing the Hamiltonian to a sum of expressions describing independent $\{Fe_3\}$ triangle and $\{Fe_6\}$ fragments. This allowed us to diagonalize the quantum Heisenberg Hamiltonian, given by Equation (1) of the separate fragments. The best fit to the susceptibility data using this quantum model gave $J_a = -173.7$ cm⁻¹, $J_b = -30.9$ cm⁻¹, and $J_c = -19.1$ cm⁻¹. The measured $\chi_M T$ curve, and the calculated values using the quantum model of two decoupled fragments are shown in Figure 3.

In the low-temperature limit the ground state for the $\{Fe_6\}$ portion has $S = 0$, but the ground state of the $\{Fe_3\}$ triangle is a pair of degenerate $S = 1/2$ states. The assumption of negligible exchange between the two sections of the structure leads to an $S = 1/2$ ground state for the entire $\{Fe_9\}$ cage. This interpretation is strongly supported by the fact that the low-temperature theoretical limit of $\chi_M T$ for the system, in emu K mol⁻¹, is $0.1246g^2 S(S+1) = 0.374$ for $S = 1/2$ and $g = 2$, in very good agreement with the low-temperature limit of the experimental data, 0.38 ± 0.02, as obtained by quadratic

polynomial interpolation of the experimental data in the range 2–20 K (see inset of Figure 3). The relevant excited levels (in zero field) of the {Fe$_6$} portion are a pair of $S=1$ levels (total degeneracy $2(2S+1)=6$) at 8.1 cm^{-1} and a pair of $S=2$ levels (total degeneracy of 10) at 36.9 cm^{-1} above the ground state. The resulting implications for the behavior of the magnetization in strong magnetic fields are given in the following subsection. For the {Fe$_3$} triangle the energy gap to the first excited level is 260 cm^{-1} and therefore this excited level is of no relevance in the following.

The very small discrepancy seen in the inset of Figure 3 below 5 K is probably due to the assumption that the six- and three-spin fragments are completely decoupled, that is, $J_2=0$. While introducing a nonzero value of J_2 might in principle provide a somewhat improved fit below 5 K, matrix diagonalization of the resulting Hamiltonian is impractical using available computational facilities. Although some of us have used quantum Monte Carlo methods to interpret magnetic data[14] this technique is not applicable here as frustration will prevent the calculations from converging due to large statistical errors.

High-field magnetic studies: The above picture of two independent fragments and the specific numerical values of the exchange constants is also supported by the behavior of the magnetization, M, versus external fields up to 50 T for the temperature $T=70$ mK (Figure 5). The behavior is slightly

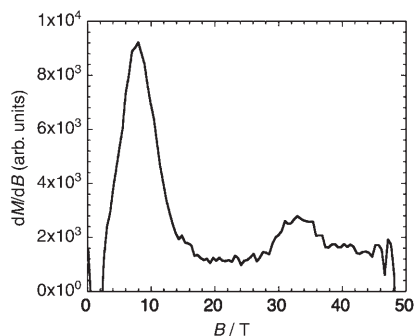Figure 5. dM/dB for **1** measured at 70 mK.

hysteretic; the data shown are for decreasing field. Using the energy levels of the {Fe$_6$} section of the structure and including a Zeeman term with $g=2$ the quantum model predicts that with increasing field the first ground-state level crossing occurs at 8.5 T (intersection of the $|S=0,M=0>$ and $|S=1,M=-1>$ levels). The next ground state level crossing (intersection of the $|1,-1>$ and $|2,-2>$ levels) occurs at 31.0 T. The behavior of the measured differential susceptibility is in very good agreement with these predictions, showing peaks at fields of approximately 9 and 33 T, respectively. The breadth of the experimental peaks could be due to a spread of exchange values.

Phonon bottleneck effect: In Figure 6 is shown the magnetization obtained upon cycling the external field through a
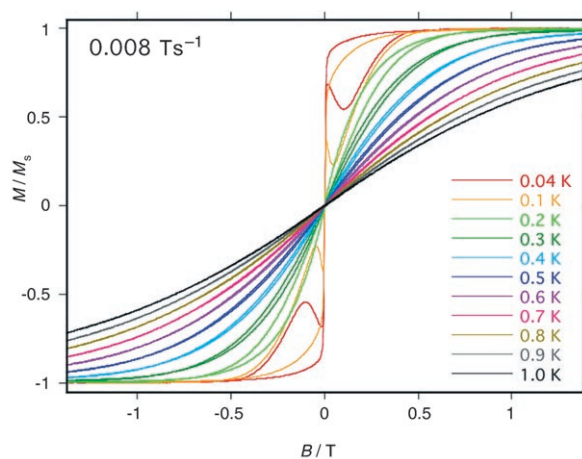
Figure 6. M against H for a crystal of **1** measured at a sweep rate of 0.008 T s^{-1} at various temperatures.

closed loop at a fixed rate of 0.008 T s^{-1} for a series of temperatures from 40 mK to 1 K. The hysteretic behavior can be attributed to the weak coupling at very low temperatures of the instantaneous magnetization of the {Fe$_3$} fragment to lattice phonon modes: often called a "phonon bottleneck".[15] Similar behavior has been observed in a {V$_{15}$} cage with an $S=1/2$ ground state,[16] in a {Cr$_{12}$} cage with an $S=6$ ground state,[17] in a {Cr$_7$Ni} antiferromagnetically coupled ring[18] and in a {V$_6$} cage which contains two weakly coupled triangles each of which has an $S=1/2$ ground state.[19] The magnetization reversal seen in the vicinity of $H=0$ is a Landau–Zener–Stückelberg (LZS) transition, and this provides further evidence of the $S=1/2$ character of the ground state.

Perhaps the most striking feature of the curves is the non-monotonic behavior of the magnetization at the lowest temperatures. The sharp local maxima and minima arise from the nonlinear coupling of the magnetization with the phonon modes. Complementary information is provided by the curves measured at $T=40$ mK for a series of different sweep rates (Figure 7). The present system thus provides an attractive platform for the development of a quantitative study of dynamical hysteresis, the LZS transition, and the phonon bottleneck effect. One of us has recently developed a general quantitative theory[20] to account for such phenomena. Efforts to apply this theory to the present system are underway but a variety of possible scenarios remain to be examined.

Microwave absorption experiments: The sample within the micro-SQUID array was also irradiated with variable frequency microwaves (between 1 and 11.4 GHz). Similar experiments performed on a {Cr$_7$Ni} AF-wheel have been reported previously.[21] The result is absorption of energy by the $S=1/2$ ground state as in an EPR experiment (Figure 8). The result is that a single absorption peak at low fields and frequencies is split into a pair of peaks with spacing propor-
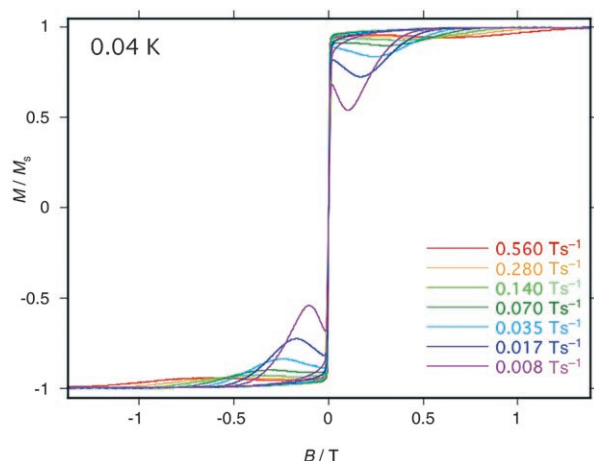
Figure 7. M against H for a crystal of **1** measured at 0.04 K and at various sweep rates.
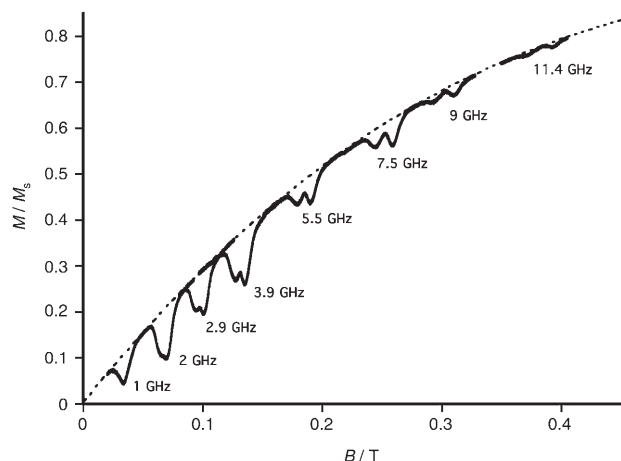

Figure 8. Change of magnetization of a crystal of **1** measured at 0.04 K, on irradiation with microwaves of the frequencies shown.

Figure 9. The EPR spectrum of a powder of **1** measured at 5 K and at a) 3.9 and b) 24 GHz.

tional to magnetic field. Analysis of this data indicates a pair of g values with $g = 2.07$ and 2.19.

A conventional EPR experiment was performed on a powdered sample at both 3.9 and 24 GHz at 5 K (Figure 9). At the higher frequency the resonance looks like an axial $S = 1/2$ species, with g_{eff} values of 2.25 and 2.03; the high field side of this resonance is rather broad, probably indicating the presence of another absorption. At the lower frequency, similar to that used in the micro-SQUID experiment, we see the same pair of g_{eff} values (much less well-resolved) but also a broad feature at $g_{eff} = 1.79$. This feature may be the broad feature on the high field side of the $g = 2.03$ signal in the 24 GHz spectrum. The g values found for the single-crystal measurements within the micro-SQUID lie between the extremes found in the powder measurements at both 3.9 and 24 GHz, and therefore the results are consistent with one another.
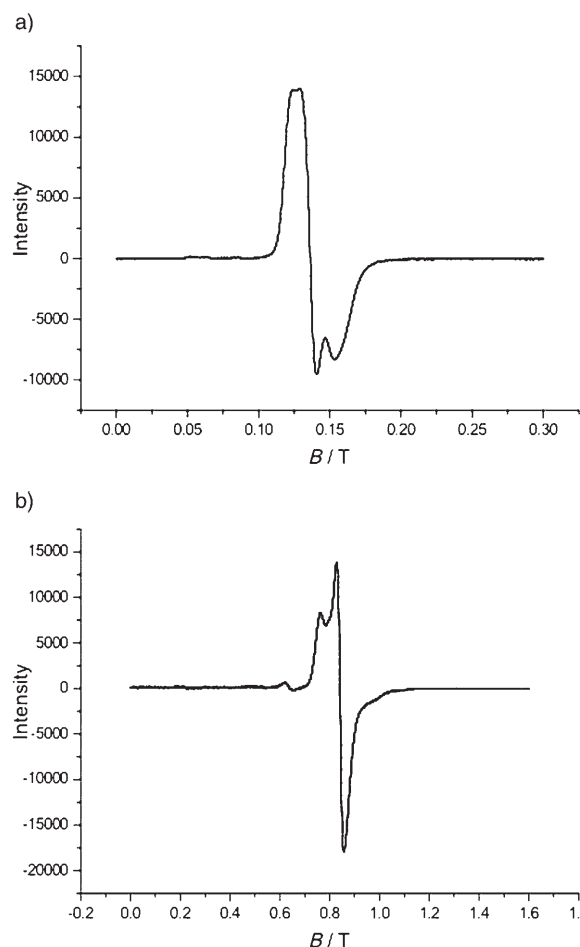
Such highly anisotropic g_{eff} values have been seen in studies of Fe^{III} oxo-centered triangles. In principle the ground state is a degenerate pair of $S = 1/2$ states, however the anti-symmetric Dzyaloshinsky–Moria interaction lifts the degeneracy. This causes all the wavefunctions to be mixed, therefore the EPR transitions are not intra-doublet, that is, due to individual $S = 1/2$ states.[22] Therefore these are not genuine molecular g values. Work by Yablokov et al. allows us to estimate the energy gap between the two $S = 1/2$ states from the observed EPR spectra,[22] making the assumptions that g is isotropic and 2.003, and that the triangle is equilateral. The calculated energy gap for **1** is 0.05 cm^{-1}. We can then assign the central resonance at $g_{eff} = 2.003$ as due to transitions when the field is perpendicular to the non-crystallographic C_3 axis of the triangle, and the resonances at $g_{eff} = 2.25$ and 1.79 as due to transitions when the field is parallel to the C_3 axis.

Discussion

One of the most recognizable features of an icosahedron is the presence of pentagonal faces and therefore the ability of the phosphonate ligand to adopt the 5.221 bonding mode is key to the formation of the tridiminished icosahedron because it produces iron(III) pentagons. This is related to the argument made by Müller et al. that the presence of pentagons is vital in the formation of nanoscale polyoxometalate cages;[23] in those clusters {Mo₆} fragments provide the pentagons. If trioxo ligands such as phosphonates can also generate pentagonal metal arrays this suggests a route worth exploring towards larger structures.

To complete the Platonic solid we need to replace the three P atoms in **1** by paramagnetic centers; use of a "complex ligand" that has three terminal oxo bridges is required. A dinuclear iron(III) complex is known which contain three μ-hydroxo groups, for example, [Fe₂(μ-OH)₃(Me₃tacn)₂];[24] whether mononuclear fragments related to this dimer can be generated and then used in place of phosphonates in **1** is debatable, but it seems a worthy synthetic target as we strive to achieve an icosahedron.

The diverse measurements reported here are all consistent with each other, and with the picture that the magnetic response of the individual cluster can be pictured in terms of the independent contributions of an {Fe₆O₃} section, with an $S=0$ ground state, and an {Fe₃O} triangle with $S=1/2$. This simple picture was first arrived at by our qualitative analysis of possible exchange paths. The very good quantitative agreement achieved between experiment and theory for the temperature dependence of $\chi_M T$ and the field dependence of dM/dB provides confidence in using the Heisenberg Hamiltonian of Equation (1) and the specific numerical values chosen for the various exchange constants. We will in the future attempt to obtain direct information on the magnetic energy levels, for example by inelastic neutron scattering. The availability of such information would at the very least provide an independent check of the form of the spin Hamiltonian model for this cluster. We also hope to provide a quantitative interpretation of the phonon-bottleneck effect.

Experimental Section

Synthesis: [Fe₃O(O₂CCMe₃)₆(H₂O)₃](O₂CCMe₃)·2HO₂CCMe₃ was made by a literature method.[25]

1·Et₂O: MeCN (30 mL) was added to [Fe₃O(O₂CCMe₃)₆(H₂O)₃]-(O₂CCMe₃)·2Me₃CCO₂H (2.3 g, 2.0 mmol) and PhPO₃H₂ (0.32 g, 2.0 mmol) and the mixture stirred for 24 h, leading to dissolution of starting materials and precipitation of a brown powder. The powder was collected by filtration and washed with MeCN until the washing solution became yellow. The residual solid was dissolved in Et₂O (50 mL), filtered, and Et₂O diluted with MeCN (25 mL). Concentration of the solution by slow evaporation at ambient temperature in five days gave large brown crystals of **1** suitable for an X-ray study. Compound **1** was filtered, washed with MeCN, and dried in air. Yield: 1.1 g (68% based on Fe) Elemental analysis (%): calcd for **1·Et₂O** (C₈₇H₁₄₂Fe₉O₄₀P₃): C 43.12, H 5.91, Fe 20.74, N 0.0, P 3.83; found: C 43.14, H 6.12, Fe 20.73, N 0.0, P 3.91.

Crystallography: Crystal data and data collection and refinement parameters for **1** are given in Table 1; selected bond lengths and angles are given in Table 2.

Data collection and processing: Data were collected with a Bruker Smart Apex CCD area detector equipped with an Oxford Cryosystems low-temperature device,[26] using Mo$_{K\alpha}$ radiation. Complete hemispheres or

Table 1. Experimental data for the X-ray study of compound **1**.

formula	C₈₇H₁₃₂Fe₉O₄₀P₃
M	2413.5
crystal system	monoclinic
space group	Cc
a [Å]	24.5904(12)
b [Å]	20.5709(10)
c [Å]	22.0099(10)
β [°]	94.4490(10)
U [Å]	11 100.1(9)
T [K]	100(2)
Z	4
ρ [g cm⁻¹]	1.444
shape and color	brown plate
size [mm]	0.2×0.2×0.1
μ [mm⁻¹]	1.262
unique data	24 995
absorption correction	SADABS
transmission max/min	0.8842, 0.7864
unique data [$F_o > 4\sigma F_o$]	5467
parameters/restraints	1043/0
$R1$, $wR2$[a]	0.0493, 0.1047
weighting scheme[b] [w^{-1}]	$\sigma^2(F_o^2) + (0.0363P)^2$
goodness of fit	0.916
largest residuals [e Å⁻³]	+0.903, −0.596

[a] $R1$ based on observed data, $wR2$ on all unique data. [b] $P=1/3[\max(F_o^2,0) + 2F_c]$.

spheres of data were collected using $\varphi\omega$ scans (0.3°, up to 30 seconds/frame). Integrated intensities were obtained with SAINT+.[6] Data were corrected for Lorentz and polarization factors, and for absorption.

Structure analysis and refinement: The structure was solved by direct methods using SHELXS-97[27] and completed by iterative cycles of ΔF syntheses and full-matrix least-squares refinement. All non-H atoms were refined anisotropically. All H atoms were included in idealized positions. All refinements were against F^2 and used SHELXL-97.[27]

CCDC-237226 contains the supplementary crystallographic data for this paper. These data can be obtained free of charge from the Cambridge Crystallographic Data Centre via www.ccdc.cam.ac.uk/data request/cif.

Measurements: Magnetic susceptibility measurements were performed on polycrystalline samples in the temperature range 2.0 to 298 K in applied fields of 0.1, 0.5, and 1.0 T using a Quantum Design MPMS SQUID magnetometer. Corrections for diamagnetic contributions were applied by using Pascal's constants. The sample holder diamagnetism was measured and subtracted from the raw data. The magnetization was separately measured in pulsed magnetic fields up to 50 T (sweep rate 15000 T s⁻¹) at Okayama University (0.45 K) and Osaka University (70 mK, 1.3 K) in their high field magnetic laboratories. A home-made μ-SQUID magnetometer[28] has been used for low temperature magnetic measurements on single microcrystals of **1**.

Acknowledgements

Table 2. Selected bond lengths [Å] and angles [°] for **1**.

Fe1—O38	1.938(3)	Fe1—O16	2.028(3)	Fe1—O18	1.968(4)	Fe1—O6	2.042(3)	Fe1—O20	1.997(3)
Fe1—O7	2.055(3)	Fe2—O38	1.935(3)	Fe2—O35	2.034(3)	Fe2—O21	1.975(3)	Fe2—O1	2.049(3)
Fe2—O33	1.988(3)	Fe2—O4	2.069(3)	Fe3—O36	1.865(3)	Fe3—O25	2.003(4)	Fe3—O31	1.974(4)
Fe3—O3	2.173(3)	Fe3—O28	1.997(4)	Fe3—O9	2.243(3)	Fe4—O37	1.862(3)	Fe4—O17	2.002(3)
Fe4—O14	1.979(3)	Fe4—O7	2.159(3)	Fe4—O10	1.997(3)	Fe4—O6	2.249(3)	Fe5—O39	1.928(3)
Fe5—O11	2.013(3)	Fe5—O37	1.933(3)	Fe5—O12	2.034(3)	Fe5—O5	1.997(3)	Fe5—O27	2.159(4)
Fe6—O39	1.915(3)	Fe6—O24	2.035(4)	Fe6—O36	1.937(3)	Fe6—O23	2.045(4)	Fe6—O2	1.995(3)
Fe6—O27	2.147(4)	Fe7—O37	1.947(3)	Fe7—O30	2.038(4)	Fe7—O8	1.972(3)	Fe7—O15	2.060(4)
Fe7—O36	1.975(3)	Fe7—O26	2.067(4)	Fe8—O38	1.944(3)	Fe8—O29	2.032(3)	Fe8—O32	1.980(4)
Fe8—O9	2.040(3)	Fe8—O19	1.986(3)	Fe8—O3	2.042(3)	Fe9—O39	1.838(3)	Fe9—O13	1.999(4)
Fe9—O22	1.965(3)	Fe9—O4	2.144(3)	Fe9—O34	1.982(3)	Fe9—O1	2.247(3)		
O38-Fe1-O18	96.29(14)	O38-Fe2-O21	96.40(14)	O38-Fe1-O20	95.40(14)	O38-Fe2-O33	95.02(14)	O18-Fe1-O20	90.41(15)
O21-Fe2-O33	90.39(15)	O38-Fe1-O16	177.43(14)	O18-Fe1-O16	83.41(14)	O38-Fe2-O35	176.33(14)	O21-Fe2-O35	82.51(14)
O20-Fe1-O16	82.06(14)	O33-Fe2-O35	81.50(14)	O38-Fe1-O6	95.00(14)	O38-Fe2-O1	96.02(14)	O18-Fe1-O6	165.75(15)
O21-Fe2-O1	164.81(14)	O20-Fe1-O6	97.17(14)	O33-Fe2-O1	97.20(14)	O16-Fe1-O6	85.70(14)	O35-Fe2-O1	85.62(14)
O38-Fe1-O7	96.66(14)	O38-Fe2-O4	97.13(13)	O18-Fe1-O7	92.40(14)	O21-Fe2-O4	91.25(14)	O20-Fe1-O7	167.24(15)
O33-Fe2-O4	167.48(14)	O16-Fe1-O7	85.90(13)	O35-Fe2-O4	86.41(13)	O6-Fe1-O7	77.64(13)	O1-Fe2-O4	78.55(13)
O36-Fe3-O31	94.54(15)	O37-Fe4-O14	100.60(15)	O36-Fe3-O28	178.88(16)	O37-Fe4-O10	89.81(14)	O31-Fe3-O28	84.34(15)
O14-Fe4-O10	91.16(14)	O36-Fe3-O25	94.82(15)	O37-Fe4-O17	173.14(15)	O31-Fe3-O25	90.97(15)	O14-Fe4-O17	84.74(14)
O28-Fe3-O25	85.32(15)	O10-Fe4-O17	85.74(14)	O36-Fe3-O3	95.10(13)	O37-Fe4-O7	92.27(14)	O31-Fe3-O3	168.95(14)
O14-Fe4-O7	89.65(13)	O28-Fe3-O3	85.99(13)	O10-Fe4-O7	177.58(14)	O25-Fe3-O3	93.57(14)	O17-Fe4-O7	92.07(13)
O36-Fe3-O9	96.27(14)	O37-Fe4-O6	95.85(14)	O31-Fe3-O9	102.64(14)	O14-Fe4-O6	155.26(13)	O28-Fe3-O9	83.88(14)
O10-Fe4-O6	107.34(13)	O25-Fe3-O9	161.66(14)	O17-Fe4-O6	80.54(13)	O3-Fe3-O9	70.94(12)	O7-Fe4-O6	71.24(12)
O39-Fe5-O37	95.27(14)	O39-Fe6-O36	96.19(14)	O39-Fe5-O5	93.76(14)	O39-Fe6-O2	91.13(14)	O37-Fe5-O5	96.72(14)
O36-Fe6-O2	100.90(14)	O39-Fe5-O11	173.15(15)	O39-Fe6-O24	174.89(15)	O37-Fe5-O11	87.32(14)	O36-Fe6-O24	88.15(14)
O5-Fe5-O11	92.22(14)	O2-Fe6-O24	85.40(15)	O39-Fe5-O12	91.46(14)	O39-Fe6-O23	91.46(14)	O37-Fe5-O12	172.78(15)
O36-Fe6-O23	169.57(14)	O5-Fe5-O12	85.43(14)	O2-Fe6-O23	85.98(14)	O11-Fe5-O12	85.71(14)	O24-Fe6-O23	84.57(14)
O39-Fe5-O27	77.42(14)	O39-Fe6-O27	77.98(14)	O37-Fe5-O27	92.58(14)	O36-Fe6-O27	90.65(14)	O5-Fe5-O27	167.75(14)
O2-Fe6-O27	164.98(15)	O11-Fe5-O27	96.17(14)	O24-Fe6-O27	104.72(15)	O12-Fe5-O27	86.32(14)	O23-Fe6-O27	84.01(15)
O37-Fe7-O8	97.41(14)	O38-Fe8-O32	95.64(14)	O37-Fe7-O36	88.41(14)	O38-Fe8-O19	94.64(14)	O8-Fe7-O36	95.67(14)
O32-Fe8-O19	90.89(15)	O37-Fe7-O30	176.52(15)	O38-Fe8-O29	175.72(14)	O8-Fe7-O30	85.88(14)	O32-Fe8-O29	82.03(14)
O36-Fe7-O30	90.15(14)	O19-Fe8-O29	81.84(14)	O37-Fe7-O15	91.20(14)	O38-Fe8-O9	97.26(14)	O8-Fe7-O15	83.53(14)
O32-Fe8-O9	164.85(15)	O36-Fe7-O15	179.06(14)	O19-Fe8-O9	95.96(14)	O30-Fe7-O15	90.29(14)	O29-Fe8-O9	85.57(14)
O37-Fe7-O26	97.89(15)	O38-Fe8-O3	95.92(14)	O8-Fe7-O26	158.38(14)	O32-Fe8-O3	93.02(15)	O36-Fe7-O26	99.94(14)
O19-Fe8-O3	168.32(14)	O30-Fe7-O26	79.24(15)	O29-Fe8-O3	87.80(13)	O15-Fe7-O26	80.96(14)	O9-Fe8-O3	77.78(13)
O39-Fe9-O22	95.77(15)	O34-Fe9-O4	87.27(14)	O39-Fe9-O34	173.50(15)	O13-Fe9-O4	94.45(13)	O22-Fe9-O34	87.24(14)
O39-Fe9-O1	88.37(14)	O39-Fe9-O13	98.20(14)	O22-Fe9-O1	100.80(14)	O22-Fe9-O13	91.25(15)	O34-Fe9-O1	85.40(13)
O34-Fe9-O13	87.47(14)	O13-Fe9-O1	165.66(13)	O39-Fe9-O4	89.12(14)	O4-Fe9-O1	72.81(12)	O22-Fe9-O4	171.90(14)
Fe6-O27-Fe5	92.20(14)	Fe3-O36-Fe6	118.13(17)	Fe2-O38-Fe1	120.08(17)	Fe3-O36-Fe7	118.66(17)	Fe2-O38-Fe8	120.02(16)
Fe6-O36-Fe7	122.97(16)	Fe1-O38-Fe8	119.63(17)	Fe4-O37-Fe5	118.44(17)	Fe9-O39-Fe6	124.10(18)	Fe4-O37-Fe7	118.91(18)
Fe9-O39-Fe5	121.98(17)	Fe5-O37-Fe7	121.33(17)	Fe6-O39-Fe5	107.70(16)				

[1] Plato, *Timaeus*, (trans. D. J. Zeyl), Hackett Publishing Company, Indianapolis USA, **2000**, pp. 45–46.

[2] R. E. P. Winpenny, *Adv. Inorg. Chem.* **2001**, *52*, 1–111.

[3] C. Schröder, H.-J. Schmidt, J. Schnack, M. Luban, *Phys. Rev. Lett.* **2005**, *94*, 207203–207206.

[4] E. I. Tolis, M. Helliwell, S. Langley, J. Raftery, R. E. P. Winpenny, *Angew. Chem.* **2003**, *115*, 3934–3938; *Angew. Chem. Int. Ed.* **2003**, *42*, 3804–3808.

[5] A. Bino, I. Shweky, S. Cohen, E. R. Bauminger, S. J. Lippard, *Inorg. Chem.* **1998**, *37*, 5168–5172.

[6] W. Schmitt, C. E. Anson, W. Wernsdorfer, A. K. Powell, *Chem. Commun.* **2005**, 2098–2100.

[7] L. K. Thompson, L. Zhao, Z. Xu, D. O. Miller, W. M. Reiff, *Inorg. Chem.* **2003**, *42*, 128–139.

[8] Harris notation describes the binding mode as $[X.Y_1Y_2Y_3\cdots Y_n]$, where X is the overall number of metals bound by the whole ligand, and each value of Y refers to the number of metal atoms attached to the different donor atoms. See: R. A. Coxall, S. G. Harris, D. K. Henderson, S. Parsons, P. A. Tasker, R. E. P. Winpenny, *Dalton Trans.* **2000**, 2349–2356.

[9] The Johnson solids are uncommon polyhedra. A list is given at: http://mathworld.wolfram.com..

[10] L. A. Welo, *Philos. Mag.* **1928**, *6*, 481–488.

[11] R. D. Cannon, R. P. White, *Prog. Inorg. Chem.* 195–298.

[12] Gaussian 98, Revision A.11.3, M. J. Frisch, G. W. Trucks, H. B. Schlegel, G. E. Scuseria, M. A. Robb, J. R. Cheeseman, V. G. Zakrzewski, J. A. Montgomery, Jr., R. E. Stratmann, J. C. Burant, S. Dapprich, J. M. Millam, A. D. Daniels, K. N. Kudin, M. C. Strain, O. Farkas, J. Tomasi, V. Barone, M. Cossi, R. Cammi, B. Mennucci, C. Pomelli, C. Adamo, S. Clifford, J. Ochterski, G. A. Petersson, P. Y. Ayala, Q. Cui, K. Morokuma, N. Rega, P. Salvador, J. J. Dannenberg, D. K. Malick, A. D. Rabuck, K. Raghavachari, J. B. Foresman, J. Cioslowski, J. V. Ortiz, A. G. Baboul, B. B. Stefanov, G. Liu, A. Liashenko, P. Piskorz, I. Komaromi, R. Gomperts, R. L. Martin, D. J. Fox, T. Keith, M. A. Al-Laham, C. Y. Peng, A. Nanayakkara, M. Challacombe, P. M. W. Gill, B. Johnson, W. Chen, M. W. Wong, J. L. Andres, C. Gonzalez, M. Head-Gordon, E. S. Replogle, J. A. Pople, Gaussian, Inc., Pittsburgh PA, **2002**.

[13] a) E. Ruiz, J. Cano, S. Alvarez, A. Caneschi, D. Gatteschi, *J. Am. Chem. Soc.* **2003**, *125*, 6791–6794; b) G. Rajaraman, J. Cano, E. K. Brechin, E. J. L. McInnes, *Chem. Commun.* **2004**, 1476–1477.

[14] L. Engelhardt, M. Luban, *Phys. Rev. B* **2006**, *73*, 054430–054438.

[15] A. Abragam, B. Bleaney, *Electron Paramagnetic Resonance of Transition Metal Ions*, Clarendon Press, Oxford **1970**, Chapter 10.

[16] I. Chiorescu, W. Wernsdorfer, A. Müller, H. Bögge, B. Barbara, *Phys. Rev. Lett.* **2000**, *84*, 3454–3457.

[17] D. Collison, M. Murrie, V. S. Oganesyan, S. Piligkos, N. R. J. Poolton, G. Rajaraman, G. M. Smith, A. J. Thomson, G. A. Timco, W. Wernsdorfer, R. E. P. Winpenny, E. J. L. McInnes, *Inorg. Chem.* **2003**, *42*, 5293–5303.

[18] W. Wernsdorfer, D. Mailly, G. A. Timco, R. E. P. Winpenny, *Phys. Rev. B* **2005**, *72*, 060409/1–060609/4.

[19] I. Rousochatzakis, Y. Ajiro, H. Mitamura, P. Kögerler, M. Luban, *Phys. Rev. Lett.* **2005**, *94*, 147204–147207.

[20] I. Rousochatzakis, M. Luban, *Phys. Rev. B* **2005**, *72*, 134424/1–134424/11.

[21] W. Wernsdorfer, D. Mailly, G. A. Timco, R. E. P. Winpenny, *Phys. Rev. B* **2005**, *72*, 060409/1–060409/4.

[22] Yu V. Yablokov, V. A. Gaponenko, V. V. Zelentsov, K. M. Suvorova, *Solid State Commun.* **1974**, *14*, 131–135.

[23] A. Müller, P. Kögerler, A. W. M. Dress, *Coord. Chem. Rev. 2001, 222*, 193–218.

[24] S. Druëke, P. Chaudhuri, K. Pohl, K. Wieghardt, X. Q. Ding, E. Bill, A. Sawaryn, A. X. Trautwein, H. Winkler, S. J. Gurman, *J. Chem. Soc. Chem. Commun.* **1989**, 59–62.

[25] A. S. Batsanov, Yu. T. Struchkov, G. A. Timko. *Koord. Khim.* **1988**, *14*, 266–270.

[26] J. Cosier, A. M. Glazer, *J. Appl. Crystallogr.* **1986**, *19*, 105–107.

[27] SHELX-PC Package, Bruker Analytical X-ray Systems, Madison, WI, **1998**.

[28] W. Wernsdorfer, *Adv. Chem. Phys.* **2001**, *118*, 99–192.